Optical Elements for a CMBPol Mission

Editors: H. Tran[1] & L. Page[2]

[1] Dept. of Physics, University of California, Berkeley
[2] Dept. of Physics, Princeton University

E-mail: huantran@berkeley.edu

Abstract. We present an overview of selected optical technologies that are candidates for use in the CMBPOL satellite mission, indicate how the technologies are being tested, and estimate their Technology Readiness Level (TRL).

1. Introduction

There are at present multiple proposed configurations for a satellite to measure the B-mode polarization of the CMB. Schemes range from bare corrugated horns aimed directly at the sky[1] to 2 m reflector telescopes[2], and include interferometers[3] and smaller reflector/refractor systems. Each optical configuration is optimized for a specific scientific or technological purpose. We can draw on experience from COBE and WMAP (and soon PLANCK) to evaluate some technologies such as corrugated feedhorns and large composite reflectors, but there are other technological components that have not yet flown, most notably millimeter AR coatings, which may or may not be needed for a space mission.

In the next few years a number of new CMB polarization experiments will come online as shown in Table 1. The QUAD and BICEP experiments have already taken enough data to investigate the performance of on-axis reflectors and small AR coated refractors coupled to multiple corrugated feedhorns. In the next few years the launch of the EBEX and SPIDER balloon payloads is anticipated. PLANCK is planned for a 2009 launch. With the array of techniques that will be tested soon, in combination with the lessons already learned, one expects that near 2012 multiple detailed instrument designs for CMBPOL that are grounded in experience will be possible.

This paper containers a collection of studies on potential optical elements for a satellite to measure the B-mode polarization of the CMB. The contributions are organized as follows.

In each entry, the current status of optical technologies relevant to CMBPol is reviewed. Based on the author's and our read of the state of the technology we summarize here the Technological Readiness Level (TRL) of the various technologies. To be ready for a satellite proposal, the technology must have a TRL of 5.

Corrugated feeds without lenses. TRL 7. These have flown in space and there are accurate codes to model the polarization response.

Corrugated feeds with lenses. TRL 4-5. These have been used on the ground in numerous experiments though there has not been an analytic study of the polarization properties.

Corrugated feeds with dual offset reflector systems and codes to assess them. TRL 7. These have flown in space and there are accurate codes to model the polarization response.

Antenna feeds with reflectors or lenses TRL 3. Antenna based focal planes will soon be used on the ground in both lens and dual reflector systems. The tools used to simulate polarized feed patterns are still maturing.

On-axis Reflector Systems TRL 3 to 9. On-axis design using conventional rigid feedleg secondary support: TRL 9 — but does not meet requirements. On-axis design using "zero blockage" secondary support: TRL 3 — research required to prove feasibility, and may not meet requirements anyway.

Single-layer AR coatings TRL 4-5. Single layer AR coatings for large plastic and silicon lenses estimated to be at TRL 5, with the possible exception of vibration testing and radiation testing. They have been produced and are in use. They may be modeled fairly well.

Multi-layer broadband AR coatings TRL 2-3. Multi-layer broadband AR coatings for large plastic and silicon lenses are being developed and will soon be tested in the field.

Simulated dielectrics on HDPE lenses for single bands TRL 5.

Simulated dielectrics for wide bands TRL 4. Wide band tapered designs (grooves in LDPE, pyramids in flat rexolite) have been prototyped, but have not yet been fielded in CMB polarization experiments.

Simulated dielectrics for silicon TRL 2.

Table 1. CMB Polarization Experiments Post 2007[1]

Name	Status	Frequency	Optical Configuration	AR coatings
Ground:				
QUaD	Done	100&150 GHz	Feed-fed refractive receiver on an on-axis 2.6 m Cass[2]	Yes
BICEP	Observing	100&150 GHz	Feed-fed refractive receiver	Yes
QUIET	Launching	40&90 GHz	Feed fed CD[3]	No
ABS	Building	150 GHz	Feed-fed cryo 1 m CD	No
BICEP2	Building	100&150 GHz	Antenna-fed refractive receiver	Yes
CLOVER	Building	97,150,&225 GHz	Feed-fed 1.8 m CD	No
MBI	Building	90 GHz	Bolometric Interferometer	No
POINCARE	Building	40 & 150 GHz	CD	No
POLARBEAR	Building	150& 220 GHz	Greg[4]/ Refractor	Yes
ACTPOL	Planning	TBD	TBD	TBD
SPTPOL	Planning	TBD	TBD	TBD
Balloon:				
EBEX	Building	150, 250,& 410 GHz	Greg/ Refractor	Yes
SPIDER	Building	40, 90, 145, & 220 GHz	Refractor	Yes
PAPPA	Building	89, 212, & 302 GHz	Single offset reflector	No
Current Satellite:				
WMAP	Observing	22-95 GHz	Feed-fed 1.4 m Greg	No
PLANCK	Building	30-680 GHz	Feed-fed 1.5 m Greg	No

([1]) The table focuses on just the optical components discussed in this section. There are many other distinguishing features between experiments. ([2]) Cass is for a Cassegrain reflector system. ([3]) CD stands for Crossed Dragone reflector system. ([4]) Greg is for an offset Gregorian reflector system.

2. Offset Dual reflector systems for CMBPOL by Huan Tran

2.1. Background on Offset Dual Reflector Systems

Reflector based systems are the only practical method of achieving apertures larger than ∼60 cm. Dual reflector systems have long been used in astronomy to produce either a more compact design or to produce a larger field of view (FOV). Offset dual reflector designs have the added benefit of an unobstructed aperture, leading to lower sidelobe levels. Furthermore, offset dual reflectors will have a larger FOV when compared to similar centered systems with small obstructions. Offset systems do, however, violate circular symmetry, leading to more polarization effects. Detailed simulations show that polarization systematics induced by the reflectors is at or below the level induced by the feeds, although more investigation is necessary.

Two broad configurations of offset dual reflectors have been considered in the community, the Gregorian and the Crossed Dragone. The most common configuration is the Gregorian, shown in figure 1(b), which generally has a small secondary and a chief ray that traces a zig-zag pattern. An alternative configuration, the Crossed or Side-Fed Dragone, has received some recent attention [4, 5], particularly for apertures of ≈1.5 m. The Crossed Dragone uses a large secondary in a folded design, shown in figure 1(a), with a chief ray that crosses itself.

We discuss the relative merits of the Crossed and Gregorian Dragone configurations and indicate the possible future work needed to bring a dual reflector system to TRL 5 is considered.

2.2. Gregorian

The Gregorian is the dominant reflector configuration used in CMB experiments. The following sub-orbital experiments made use of Gregorian style optics: ACME, ACT, ARCHEOPS,

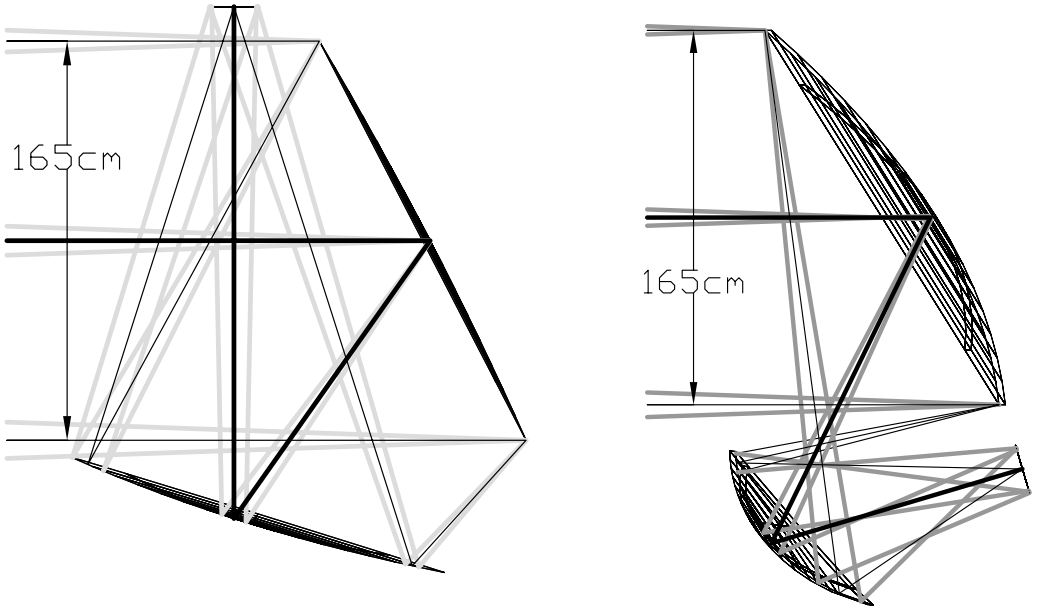

(a) Crossed (b) Gregorian

Figure 1. Diagrams of two Mizuguchi-Dragone configurations. For each, the chief ray is shown as the thick black line. The $\pm 2^\circ$ off-axis beams are shown in grey. Both have the same aperture diameter and Effective Focal Length (EFL), and thus, the same F/#. Figure taken from [6].

BOOMERANG, CAPMAP MAX, MAXIMA, SPT and VIPER. WMAP has now flown with two back to back Gregorian telescopes, and have extensively characterized the in-flight performance. The PLANCK mission will also feature a single Gregorian telescope, and they have performed a significant amount of optical analysis to ensure that the beams will perform as needed.

There are many sub-classes of Gregorian telescopes. The simplest offset Gregorian has a parabolic primary and an elliptical secondary, where the axes of symmetry of the parent conics are co-linear. A simple improvement on the design is the aplanatic, where the conic section of the primary is allowed to deviate slightly from parabolic. An alternative improvement is to allow the axes of symmetry of the primary and secondary to tilt relative to each other, satisfying the Mizugutchi-Dragone condition. Most modern CMB systems are based on these conditions, or are slightly modified from these conditions.

2.2.1. WMAP *Reflectors.* The WMAP optical systems is composed of two back-to-back 1.4 m Gregorian systems, fed by scalar feed horns. The specific configuration of the reflectors starts with the Mizuguchi-Dragone condition, and is then shaped to make the beams smaller and more symmetric [7].

The optical performance has been extensively analyzed, including figure imperfections, by comparing in-flight beams to models computed using DADRA [8]. A model for the sidelobe performance of the full satellite was also developed [9], however the theoretical simulation alone was not sufficient to model the full performance. The reason is that structural elements that affect the beam at low levels were not included in the model.

At the level that WMAP detected polarization, the optical effects were negligible [10]. The largest

effect is from a difference in the beam size and shape between the pairs of telescopes as a result of differences in telescope distortion and to passband mismatch.

The main limitation of the WMAP optics, the surface deformations, is directly traceable to the manufacturing processes for the composite optics. Other manufacturing processes have been demonstrated to result in better performance upon cooling.

2.2.2. PLANCK *Reflectors.* The PLANCK design is similar to WMAP's but instead of starting with a Mizuguchi-Dragone the base system was an aplanatic with two ellipsoidal reflectors. As with the Dragone, the axes of the two reflectors are then allowed to tilt relative to one another [11]. The resulting design provides a larger FOV than a Dragone, but has more cross polarization for the central beam.

PLANCK team members have published simulations of the telescopes. Methods have been developed to analyze the beams [12, 13] with particular attention paid to polarization performance. The key conclusion is that beam maps from orthogonal linear polarizations from a single polarization sensitive bolometer (PSB) pair within a given feedhorn should not differ by more than 0.9% in amplitude, including the effects of finite conductivity and alignment error. Beams from separate horns could differ significantly due to astigmatism induced by elliptical reflectors [14]. Thus a single non-modulated PSB horn is required to measure either Q or U. Pairs of horns are required to construct E and B. A missmatch within a horn leads to leakage from T to E and B, whereas missmatch between horns leads to leakage between E and B. The effect is largest at high ℓ, but is not negligible at low-ℓ near the gravitational wave bump.

2.2.3. Gregorian Systems with Reimaging Optics. Both WMAP and PLANCK operate without any reimaging optics. The FOV of the Gregorian telescopes is big enough to feed 10's of widely spaced detectors, and the corrugated feed horns provide enough edge taper and at the same time are individually oriented to properly illuminate the primaries.

It is unlikely that a Gregorian reflector and feedhorn system alone will have enough throughput to achieve the CMBPOL sensitivity goals. To achieve higher focal plane area utilization, the individual pixels must be smaller, leading to higher edge taper. This problem has been traditionally solved with a Lyot stop, created with reimaging optics. Some new generations of focal plane arrays also require a flat, telecentric field, also created with reimaging optics.

Reflectors have been used for reimaging optics in both BOOMERANG and MAXIMA. As throughput grows and F/# shrinks, however, reimaging with reflectors becomes more difficult because of the limited amount of space for folded beams to clear obstructions. Cold lenses are the natural solution, but they are not without their own problems.

The millimeter-wave Gregorian telescopes with cold reimaging lenses include ACT, SPT and GREEN BANK with POLARBEAR and EBEX to soon follow. For the EPIC mission concept study, a large 3 m system with large silicon reimaging optics was designed. While all designs produce large throughput at acceptable levels of optical performance, all systems are still in the initial operational phase, and the full polarization performance has yet to be determined.

2.3. Crossed Dragone.

A promising offset dual reflector configuration is the Crossed Dragone, also known as the Compact Range Antenna, or side fed antenna. This configuration has been chosen for QUIET , CLOVER and ABS , although many other experiments have seriously considered it. The biggest advantage of this configuration is the 2× larger FOV, as shown in figure 2. The Crossed Dragone has the added advantage of having a distant exit pupil, meaning that the bare focal plane is already near telecentric (see figure 1(a)). QUIET , CLOVER and ABS plan on using the Crossed Dragone without remimaging optics, relying instead on scalar feedhorns to taper the illumination at the edge

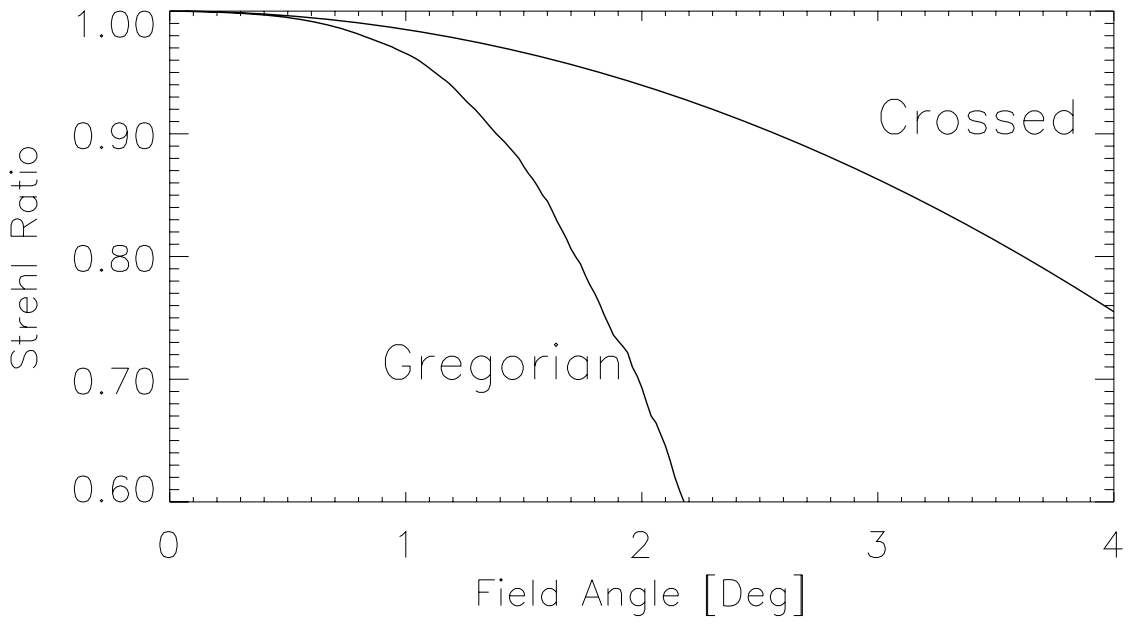

Figure 2. Strehl ratios across the focal plane, calculated at 150 GHz. The Crossed Dragone shows a clear advantage in terms of DLFOV. A design is considered diffraction limited if the Strehl ratio is above 0.8. Figure taken from [6].

of the primary. The absence of reimaging optics is a major simplification over equivalent Gregorian systems, allowing an accurate simulation of optical performance using tools such as `DADRA` and `GRASP9`.

The Crossed Dragone does suffer from a few disadvantages. Gregorian systems are more mature. A thorough design study of a Crossed Dragone configuration for a satellite mission has not yet been performed, but will be a major topic of the next phase of the CMBPol mission study.

The reflectors on a Crossed Dragone are more shallow and possibly easier to fabricate than those of the Gregorian design. The Crossed Dragone, however, does have a large secondary reflector, which makes large telescopes ($\sim$2 m and above) impractical. The large secondary also places some difficult constraints for mounting within a rocket shroud. Packing constraints will likely set the largest diameter possible for the Crossed Dragone configuration.

Another issue with the Crossed Dragone system is the tradeoff between F/# and beam clearance. There is a minimum practical F/# that is allowed before the beam either interferes with the primary or the secondary. This has implications for the quality of baffling the optics from stray light, and the level of expected sidelobes.

A third challenge for the Crossed Dragone system is the need for a large, cold aperture. To optimally use the available FOV, it is likely that closely packed pixels that maximize the focal plane illumination will be necessary. This leads directly to larger beams emanating from each pixel. In the Gregorian case with reimaging optics, the pixel sidelobes are truncated with a Lyot stop. Without a Lyot stop, the simplest solution to this problem is to use a large, cold, absorbing ring surrounding the entrance pupil.

2.4. Work required to reach TRL 5

2.4.1. Mechanical. The Gregorian configuration has already been flown in WMAP with composite reflectors. The PLANCK mission will also fly a composite Gregorian reflector system. The mechanical aspects of the reflectors themselves are already well past TRL 5; we estimate them near TRL 7.

The Crossed Dragone configuration is expected to require a large cold aperture. Cooling this ring down to levels that will keep bolometer loading low will pose some technical challenges, we expect to reach TRL 3 soon.

The Gregorian configuration requires dielectric lenses. While there have been many space-qualified refractive telescopes, a technology for broadband millimeter AR coatings that can survive cryogenic cycling and launch vibration has not yet been demonstrated.

2.4.2. Simulation. Understanding the full polarization systematic properties of full dual reflector systems is still, however, immature, especially when considering the tiny signals and extreme contrast of the B-mode signature. The behavior of the reflectors alone can be precisely simulated with available physical optics tools. Simulation tools for feeds, however, are at varying levels of maturity based on the technology used. Systems requiring "Detailed analysis" are categorized by NASA as TRL 2, although detailed simulation is not strictly required before bringing the system to a higher TRL.

The success of the WMAP beam modeling depended on the highly accurate physical optics simulation packages available that can analyze corrugated feed horns and highly conductive reflector surfaces. No such code is widely available to analyze the *dielectric* reimaging systems. In order to understand the role of reimaging lenses with the Gregorian configuration, physical optics simulations of dielectric lenses with account of their actual physical properties (absorption, internal reflection, polarization effects at reflection, any kinds of antireflection coatings, actual complicated shape etc) must be developed. A quasi-Gaussian beam analysis or similar "quasi-optical" extensions are inadequate to the real dielectric lens problem. Real lens properties are all significant and are all properly accounted for by the "lens physical optics" approach being developed [15].

Simulation tools for waveguide coupled corrugated feedhorns are mature. Tools for PSB's and antennas are not yet at the same level of accuracy. Tools for three dimensional structures with cold thin films or small dielectric lenses are still under development.

There is also possible work involved with simulations of beam forming elements in the focal plane. Discussion these simulations is outside the scope of this whitepaper, but possible areas of future development include advanced modeling of thin film polarized absorbtion in PSB's and advanced simulation of beam effects in lenslet-antenna coupled bolometers. The detailed polarization behavior of feed elements is relevant at the level of the B-mode signature. However, such systems are straightforward to characterize in the lab and in the field.

3. Suitability of On Axis Reflector Designs for a future CMB Polarization Space Mission by Clem Pryke.

This document will attempt to answer the question "Should on-axis reflector based designs be considered for use in a future CMB Polarization Space Mission?". This question can be re-phrased as follows: "Which is better — on-axis or off-axis?". The community consensus answer to this latter question is clear — all the up-coming generation of reflector based polarization experiments use off-axis designs, including EBEX , CLOVER , POLARBEAR , and QUIET .

On-axis designs have the following disadvantages versus off-axis:

- The blockage of the primary reflector by the secondary produces near sidelobes and a loss of aperture efficiency. Large field of view requires large secondaries making these problems worse.
- The secondary support structure scatters light to large angles producing far sidelobes (see below for experience from QUAD). In addition blockage by the secondary supports results in additional loss of aperture efficiency.
- The secondary reflector illuminates the annulus between the edge of the receiver entrance aperture and the start of the primary reflector potentially producing far sidelobes. (These effects can be reduced by putting a hole in the middle of the secondary, and/or baffling around the receiver entrance aperture.)
- Diffraction from the edge of the secondary reflector produces far sidelobes.

One therefore needs very compelling reasons to consider on-axis designs further. Dragone [16] has shown that if the angles in an offset antenna are chosen correctly, then aberrations and cross-polarization effects are the same as those in a conventional on-axis antenna with the same diameter and focal length. Excellent field of view is possible using off-axis designs [17].

The non-ideality of the polarization properties of telescope systems is normally discussed in terms of instrumental polarization and cross polarization. The former is the degree to which the optical system causes an un-polarized source to appear polarized. The latter is the rotation of the apparent polarization angle of a polarized source.

The net amount of instrumental polarization induced is related to the degree of symmetry in the optics, and hence off-axis designs generally give poorer performance. However the relevance of this statistic needs to be carefully considered — in an experiment which measures polarization through the differencing of two separate orthogonal detectors instrumental polarization is completely degenerate with the relative detector gains, which need to be calibrated to excellent precision anyway. For systems which employ polarization modulation or switching downstream of the optical system the optically induced instrumental polarization is potentially relevant. However by orienting the OMTs (or similar) symmetrically with respect to the optical system the effect can be nulled (as was done in CAPMAP).

It's not really the case but let's suppose that on-axis designs gave lower cross polarization — would that be sufficient reason to consider them further? To first order cross-pol is simply a rotation of the response angle of a given detector. To reach the required levels of accuracy for next generation experiments these angles will almost certainly need to be empirically measured anyway, rather than relying on design or model values. Therefore it is only if off-axis designs gave cross polarization which was *more unstable* that on-axis designs that the latter would have an advantage. Cross polarization is generated by curvature of the optical elements so it should be extremely stable, especially in a space environment.

The only CMB polarimeters so far to use on-axis reflector systems are COMPASS [18] and QUAD [19]. Rather than use a conventional tripod assembly both experiments supported the secondary reflector on a cone made from a foam material known to have low absorption and scattering at microwave frequencies, the idea being to have the secondary reflector effectively "float" in front of the primary. COMPASS used Styrofoam and reported adequate performance.

QUaD initially attempted to use Styrofoam but encountered severe problems obtaining sufficient mechanical stiffness and switched to a Zotefoam design. (Zotefoam is a polypropylene foam expanded using dry nitrogen.) Since Zotefoam is only available in 6' x 3' flat sheets an elaborate design was devised gluing two offset nine segment layers together using a very thin layer of adhesive. The foam adhesive laminate was measured to have scattering of $\sim 2\%$.

QUaD is the most sensitive CMB polarimeter to date for multipoles $\ell > 200$ and has reported good results [20]. Nevertheless it has some optical problems and is not a good model for future experiment. Ground pickup was encountered which is believed to be associated with scattering around the cryostat entrance window. In addition scattering by the foam cone produces a ring sidelobe at 100° from the optical axis which is highly polarized ($\sim 50\%$). The brightness of a point source located in this ring lobe is $\sim 10^{-4}$ relative to the main beam. This allows the moon to produce serious contamination, and at the sensitivity required for future experiments, the galactic plane would also be a problem.

The experience of QUaD is arguably not relevant to a space mission — likely a one piece foam cone support with much better properties could be developed. However it would only be worth considering this if truly compelling practical advantages for an on-axis design were identified. As outlined above no such in principle reasons are apparent. It doesn't seem that there are any practical or engineering based reasons either — while ground based off-axis telescopes are typically around three times more expensive than their on-axis equivalents this is due to the additional strength required from the mechanical structure to resist Earth's gravity, and hence doesn't apply in space. Off-axis telescopes have a proven record in space (e.g., WMAP), and the designs being considered for next generation space missions are no larger than the up-coming Planck mission.

3.1. Technology Readiness Level of On-axis Reflector Systems

On-axis design using conventional rigid feedleg secondary support: TRL 9 — but does not meet requirements. On-axis design using "zero blockage" secondary support: TRL 3 — research required to prove feasibility, and may not meet requirements anyway.

4. Layered Anti-Reflection Coatings by Chao-Lin Kuo

4.1. Overview

Reflections in optical systems cause loss and lead to systematic effects. To reduce these effects, optical elements can be antireflection (AR) coated by direct bonding of dielectric layers with the right thickness and index of refraction. Such an approach has been successfully applied to optical elements such as lenses, metal-mesh or bulk infrared (IR) blocking filters, half-wave plates, and the lenslets or silicon substrates that admit radiation in lithographic arrays of slot antenna-coupled bolometers. The most common lens/substrate materials include HDPE, PTFE (Teflon), silicon, quartz, and sapphire.

The concept of layered AR-coatings is quite simple, but the implementation can be tricky. The details depend on the coating materials, but the procedures usually involve (i) identifying and characterizing candidate coating materials with the right index of refraction; (ii) vacuum/thermal forming, or pre-machining of the AR layers; and (iii) for cryogenic applications, developing a bonding that is robust against multiple thermal cycles between room temperature and cryogenic temperatures. For multi-layer broadband AR coating, these procedures have to be repeated as many times as the number of layers. While the development of these processes can be costly and time consuming, once a recipe is found, layered AR-coatings can be produced significantly faster and less expensively than machining sub-wavelength structures onto the surfaces. Sections §4.2.1, §4.2.2, and §4.2.3 summarize successful recipes for single-layered AR-coatings of HDPE, PTFE, silicon, and progress in multi-layer AR coating silicon substrates.

4.1.1. Design and Modeling. The most important parameter in AR coatings is the index of refraction n of the substrates and the coating materials. Without AR coatings the reflective loss is given by $R = [(1 - n_s)/(1 + n_s)]^2$ per surface at normal incidence. The loss R is 30% for silicon ($n = 3.4$), and 4.5% for HDPE ($n = 1.54$). It is easy to show that an ideal single-layer AR coating at frequency ν is a dielectric layer with $n_c = \sqrt{n_s}$ and thickness $d = c/4n_c\nu$. Even with such ideal single-layer coating, the index of refraction dictates the working bandwidth of the coating. In Table 2 we list the index of refraction for several common dielectrics for substrates and coating.

The most convenient theoretical tool to calculate wave propagation in multiple layers of dielectrics is the characteristic matrix method, given in §1.6 of Born and Wolf [21]. This treatment includes full polarization effects and arbitrary incident angles. It assumes that light consists of plane waves, and the sample is planar and infinite. These are good approximations if the wavelength is much smaller than the radius of curvature of the lenses, the beam waist, and the sample size.

Polarization effects. It is a well known prediction of Fresnel equations that an incident plane wave at the dielectric interface is polarized. At the Brewster angle the reflected light is 100% polarized. The degree of polarization for the transmitted radiation is not as extreme, but can still be significant without AR coating. Figure 3 plots the induced polarization in the transmitted wave for a PTFE substrate at 5° and 20° with and without AR coating. The induced polarization can contribute to the instrumental polarization in some observing modes. Similarly, AR coating of the half-wave plate is often necessary because it significantly reduces artifacts associated with differential reflection in the ordinary and extraordinary axes.

4.1.2. Measurements. A reflectometer measurement is a quick and straightforward way to confirm the reduced reflection, though it is usually limited to only one frequency and room temperature. Transmission measurements with a Fourier Transform Spectrometer coupled to a broadband bolometer are necessary to understand the indices and the absorption losses, and they can be made at a wide range of frequencies. The beam incident on the samples needs to be slow enough such that the wavefront curvature is negligible. Spectra with and without the sample in the beam are usually taken. The "off" spectrum is used for calibration, which can be divided out.

Table 2. Dielectric properties of the materials for AR coating.[1]

Material	Index n	$\tan\delta$[2]
Silicon	3.42	2.2×10^{-4}
Sapphire	3.07/3.40	$2.3/1.2 \times 10^{-4}$
TMM 10i	3.13	
TMM 10	3.03	
TMM 6	2.55	
TMM 4	2.12	
TMM 3	1.81	
Quartz (Herasil)	1.87	0.001
Cirlex	1.84	0.008
Stycast 1266	1.68	0.023
HDPE	1.54	3×10^{-4}
PTFE	1.44	3×10^{-4}
Expanded PTFE[3]	1.2	

[1] Data from [22, 23, 24]
[2] At or around 150 GHz.
[3] Zitex, or Porex Mupor.

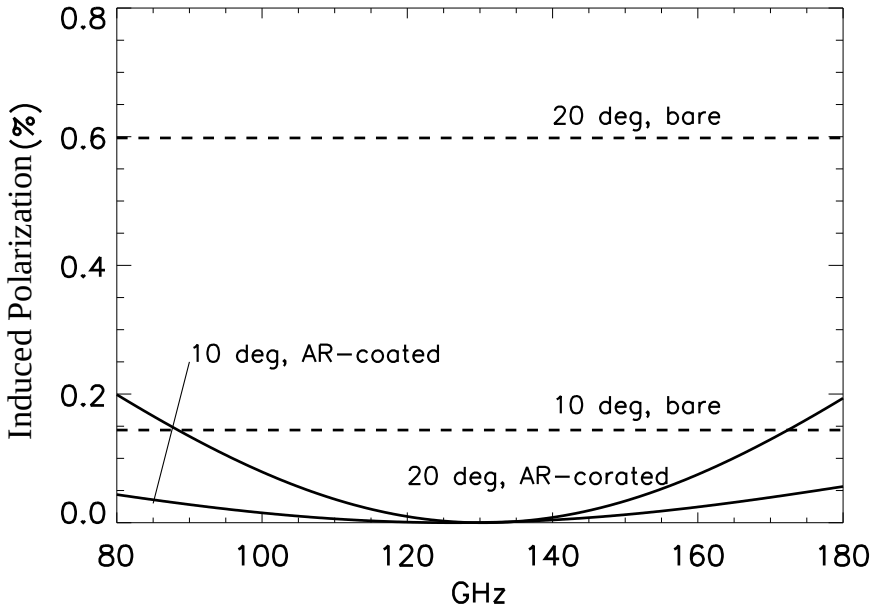

Figure 3. Induced polarization for an unpolarized plane wave transmitted through a dielectric interface, uncoated (dashed) and AR-coated (solid). The dielectric is PTFE ($n = 1.44$), and the AR coating is a single layer of expanded PTFE optimized for normal incidence at 125 GHz.

4.2. Implementation and Results.
In the next 3 sections, we describe the procedures and performance of AR coatings for HDPE, PTFE, and silicon implemented by several groups.

4.2.1. AR-Coating HDPE Lenses and PTFE Filters for BICEP The BICEP optics include 2 HDPE lenses and 2 PTFE thermal filters, all AR coated with single-layer expanded PTFE membranes using thermal lamination techniques. Without AR-coating, the IR blocking filters at LN_2 and the vapor-cooled shield (VCS) stages would have incurred over 10% loss and ghost beams at a similar level [25]. The two HDPE lenses, if left uncoated, would produce higher reflections then the PTFE filters because of the higher index ($n = 1.54$ vs 1.44). In addition, reflection from lenses cause polarized ghosting which must be reduced.

The flat PTFE filters are relatively straightforward to AR coat. Because of the low index of refraction, a single layer, $\lambda/4$ coating provides enough bandwidth for both of BICEP's frequency bands, 100 and 150 GHz. An ideal single layer coating for PTFE should have an index of $\sqrt{1.44} = 1.2$. Micro-porous PTFE (Mupor or Zitex) is an excellent material for this purpose. It has very low loss in the millimeter wave band. The manufacturers supply a variety of void fractions, pore sizes, and thicknesses. A void volume of 40% provides roughly the right index ($n \sim 1.2$) to AR coat PTFE [26]. The target thickness d is optimized for 125 GHz ($\lambda = 2.4$ mm) to cover both frequency bands. We identify the Mupor PM23DR membrane supplied by Porex Inc. to be a good approximation to the ideal $d = 2.4/4n = 0.5$ mm.

Because of their similar coefficients of thermal expansion, it is relatively straightforward to bond the Mupor membranes onto the surfaces of the filters. One slight complication in bonding PTFE is surface treatment. Because of its non-stick surface properties, the PTFE filters need to be chemically etched (Tetra-Etch) before bonding. The etching procedure changes the appearance and the color of the surface. However, the etched layer is only a few molecules thick, and no measurable increase in microwave loss is observed after etching. Two bonding techniques are tested. The first approach uses Eccobond 24 (a clear, low viscosity epoxy similar to Stycast 1266), estimated to be 0.02-0.05 mm thick, to join the substrate and the membrane. Another method uses thermal lamination, with a layer of LDPE between the substrate and membrane as the bonding film. Both methods provide excellent bonding that survives thermal cycling between room temperature and LN_2. We found it easier to apply uniform bonding for large aperture components with the heat lamination approach. (Fig. 4 a) is the measured transmission of a PTFE sample that is AR-coated on both sides with the Mupor membranes. Compared to the blank substrates (Fig. 4 b), the Fabry-Perot fringes are reduced significantly. The measured spectra agree very well with the model spectra.

We apply the same AR coating technique on the HDPE lenses and also obtain good results. An ideal single layer coating for HDPE should have an index of $\sqrt{1.54} = 1.24$, similar to the requirements for PTFE. No etching is required for bonding HDPE with Mupor membranes. However, the lamination temperature needs to be controlled accurately, because of the similarity in the melting temperatures of HDPE and LDPE. To bond Mupor membranes onto the curved lens surfaces, it is helpful to use thermal or vacuum forming techniques to pre-form the membranes into the right shape. The thermal laminations were done with an aluminum press shaped to match the lens surfaces. The coated PTFE filters and HDPE lenses have survived numerous thermal cycles.

In-band Scattering. The pores in the expanded PTFE sheet Rayleigh scatter far-IR, and to some extent, millimeter wave radiation. While scattering in short wavelengths provides additional IR blocking capability, scattering in-band can reduce efficiency and create loading from stray-light coupling. According to the vendor, the pore size of Mupor PM23DR membrane is $\sim 1.5\mu$m, and filling factor $f \sim 0.6$. To estimate the effect of Rayleigh scattering in mm-wave, we model the medium as being made of PTFE spheres with a characteristic radius of $a = 0.75\mu$m. The attenuation factor due to Rayleigh scattering [27] is given by $\alpha_R = 8\pi^3 N\gamma^2/3\lambda^4$, where N is the

number density of the "molecules", given by $3f/4\pi a^3$. The polarizability γ of a dielectric sphere is given by $\gamma = 4\pi a^3(\epsilon - 1)/(\epsilon + 2)$. From these relations and parameters, we obtain a completely negligible attenuation factor $\alpha_R \sim 2 \times 10^{-9}$ cm^{-1} at 2 mm wavelength.

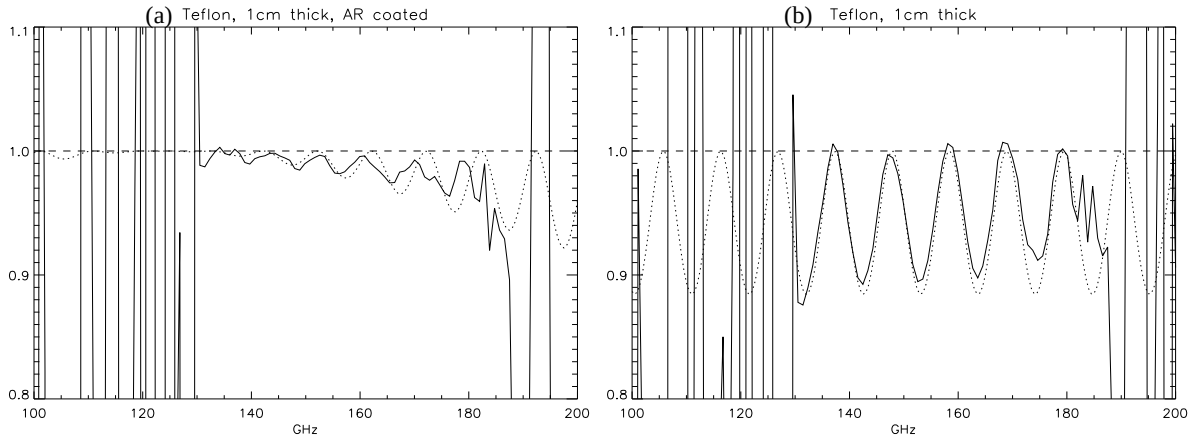

Figure 4. The transmitted spectra for a 1-cm thick PTFE sample, *left:* with Mupor AR coating, and *right:* without AR coating. The spectra are normalized by dividing by the "sample out" measurement. Outside the bandwidth of the bolometric radiometer (130 GHz - 180 GHz) the response drops to zero and the spectra become noisy. The dashed lines are the theoretical calculations assuming $n_s = 1.44$ and $n_c = 1.2$. This coating is optimized for 125 GHz but performs well for both the 100 GHz and 150 GHz bands of BICEP .

4.2.2. AR-coating Silicon Lenses for ACT A cryogenic AR coating for silicon lenses was developed for the Atacama Cosmology Telescope (ACT) [23]. The coating, a machined piece of Cirlex® [28] polyimide glued to silicon, reduces reflection to $< 1.5\%$ per lens at the design wavelength of 2 mm while maintaining $> 90\%$ transmission at $\nu < 300$ GHz. This section describes the development and performance of the coating.

The ideal AR coating at 2 mm has $d = 270\,\mu$m and an index $n_c = 1.85$. The low-frequency (~ 1 kHz) dielectric constant and loss reported in the Kapton polyimide data sheet suggest that polyimide and silicon could be combined in an AR configuration. Cirlex is a black pressure-formed laminate of Dupont Kapton® polyimide film readily available in sheets up to 60 cm square, and a variety of thicknesses. The mm-wave index and loss of Cirlex are measured both at room temperature and cryogenic temperature. Like many materials, the index of refraction increases slightly from its room temperature value of ~ 1.84 to ~ 1.95 at 5K. These measurements confirm that Cirlex is a good AR coating material for silicon.

The Cirlex layer is glued onto the silicon surface with Stycast 1266, a two-component, low viscosity epoxy made by Emerson Cuming. Silicon and Stycast 1266 thermally contract from 296 K to 4 K with $\triangle L/L = 2.2 \times 10^{-4}$ and 110×10^{-4}, respectively. Cirlex is expected to have a coefficient of thermal expansion comparable to that of a plastic, *i.e.* approximately that of Stycast 1266 and ten to one hundred times that of silicon. Differential thermal contraction often shears apart the substrate upon cooling to cryogenic temperatures. Through experimenting, the Princeton group found that if a thin layer of Lord Ap-134 adhesion promoter [29] is applied before Stycast 1266, the coating can endure multiple cryogenic cycles [23].

The transmission spectrum of a coated silicon sample is measured with an FTS. In Figure 5, the measured spectrum is shown along with a model. The measurement is the ratio of a sample to a reference spectrum, which are averages over two and six spectra, respectively. The model is determined from the measured Cirlex, Stycast, and silicon properties given in Table 2 and by

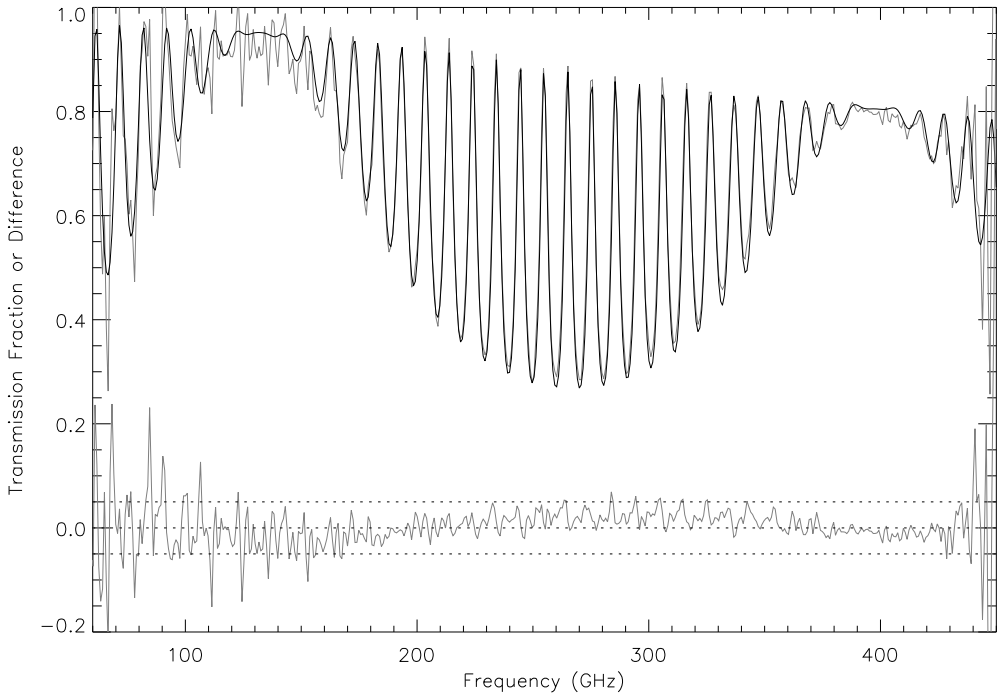

Figure 5. The room temperature transmission of a coated 4 mm-thick silicon flat, both modeled (black) and measured on the FTS (gray). The lower curve shows that the difference (measurement minus model) is within 5% of zero through the well-measured range. The slow reduction in transmittance with increasing frequency is due to increasing loss in the coating and glue [23].

measurements of the component thicknesses. The silicon loss was treated as an unknown and varied to fit the measured transmission.

For the curved lens surface, a piece of Cirlex approximately 1 cm thick is machined to the curved shape and then held in a Teflon gluing jig shaped to match the lens surface while the epoxy cures. Multiple antireflection-coated samples were made to test their robustness, including five flats—four 100 mm in diameter and one over 200 mm in diameter—and three plano-convex lenses. The lenses have been cycled four times to less than 4 K in a dewar, also without damage. The silicon lenses in ACT are all AR-coated using the procedure described here. They have been thermal cycled multiple times to 300 mK and have again shown no sign of damage.

4.2.3. Broadband AR-Coating of Silicon The CMBPol mission may well to require broadband AR coating of silicon, either for the large throughput re-imaging optics or for the focal plane arrays, depending on the details of the design. The UC Berkeley group has been developing a multi-layer AR coating for silicon using TMM, a Rogers Corporation product. TMM is commercially available as rigid sheets in a series of dielectric constants, listed in Table 2. A coating made from flat pieces of TMM and an additional layer of Zitex (expanded Teflon) was theoretically calculated to reduce percentage reflection from 30% to 3% at each silicon-vacuum interface, integrated over the three bands at 90, 150, and 220 GHz.

In a prototype testing, AR coatings were applied to two sides of a flat silicon sample. The transmittance spectrum is measured at 1.2 K in a light-pipe coupled FTS. The AR coating consisted of three layers of TMM and one layer of Zitex. The transmittance spectra of coated and bare silicon are shown in Figure 6. The silicon data exhibits periodic Fabry-Perot interference. The presence

of the sample introduces coupling which causes peaks in excess of 100%. The location of these peaks in frequency space is dependent on sample mounting position. This geometrical effect can also be seen in the peak and trough heights of the bare silicon data. It is apparent however that the Fabry-Perot interference is greatly reduced over a wide frequency range for the coated sample. Applications of this technology on curved surface are in development by thermosetting TMM on a curved form.

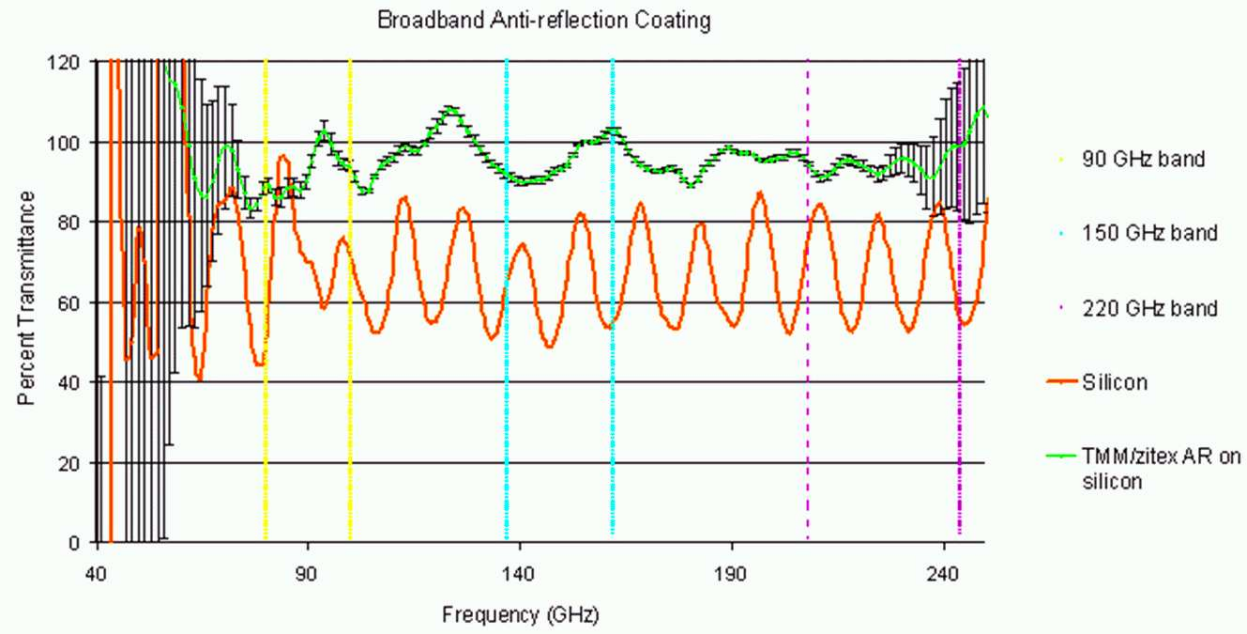

Figure 6. The transmittance spectra for a reference silicon sample and a AR-coated sample. The normalization of the measurement is affected by the optics, but the 4-layer coating significantly reduces the reflection fringes over the entire frequency range (E. Quealy).

5. Simulated Dielectric Anti-Reflection Coatings by Jeff M^{c}Mahon

It is well known that when light in a vacuum strikes a dielectric substrate with an index of refraction n at normal incidence, a fraction of the power given by $R = \left(\frac{n-1}{n+1}\right)^2$ is reflected. When light is incident at an angle θ to the normal, R depends on both θ and the linear polarization state. This leads to two issues for CMB polarization experiments. First reflected power amounts to a loss of signal which reduces sensitivity. Second, differences in the reflection coefficients for the two linear polarizations mix the Stokes parameters I, Q, and U leading to $T \rightarrow E$, $T \rightarrow B$, and $E \rightarrow B$ conversion. These effects can be reduced with AR (anti-reflection) coatings.

Several practical difficulties arise in the application of AR coatings. First, it is sometimes difficult to identify materials with the necessary index of refraction ($n' \approx \sqrt{n}$). Second, in cryogenic applications, it is necessary to match the coefficient of thermal expansion (CTE) between the matching layer and the substrate. Simulated dielectric (SD) layers offer a solution to these problems. A SD layer is manufactured by machining sub-wavelength structure into the surface of the substrate creating a layer with an effective index of refraction n' which can be tuned between n and 1.

In this note we review the principles of AR layers and then discuss the principles and technological readiness of SD-AR layers.

5.1. AR Coating Basics

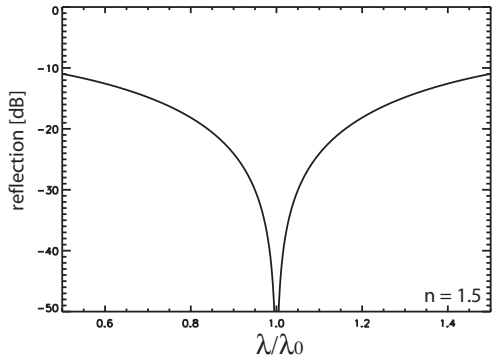

Figure 7. The reflection for a $n = 1.5$ surface AR-coated with a single layer $\lambda/4$ layer as a function of wavelength. The wavelength has been divided by the design wavelength λ_0.

The simplest AR coating consists of a $\frac{1}{4}$-wavelength ($\lambda/4$) thick layer of dielectric with index $n' = \sqrt{n}$ placed at the vacuum-dielectric boundary. The magnitude of the reflections from the front and back side of this layer are equal amplitude, and at the design wavelength, perfectly out of phase leading to a complete cancellation of the reflected power. This design is narrow-band but for $n \approx 1.5$ reflections can be suppressed below -20 dB over $\approx 20\%$ bandwidth (see Figure 7).

In many cases (e.g., lenses) it is necessary to design AR coatings that work at non-normal angles of incidence (see [30]). The angle of incidence θ is defined as the angle between the incoming ray and the local surface normal. The polarization and θ dependence of reflection and refraction from a dielectric lead to the following (different) requirements for the index of refraction of a matching layer for the two linear polarization states

$$n'^{\,2}_{||}(\theta) = \frac{n^2 + \sqrt{n^4 - 4n^2 \cos\theta \sin^2\theta \sqrt{n^2 - \sin^2\theta}}}{2\cos\theta\sqrt{n^2 - \sin^2\theta}}, \tag{1}$$

for light parallel to the plane of incidence, and

$$n'^{\,2}_{\perp}(\theta) = \sin^2\theta + \cos\theta\sqrt{n^2 - \sin^2\theta}, \tag{2}$$

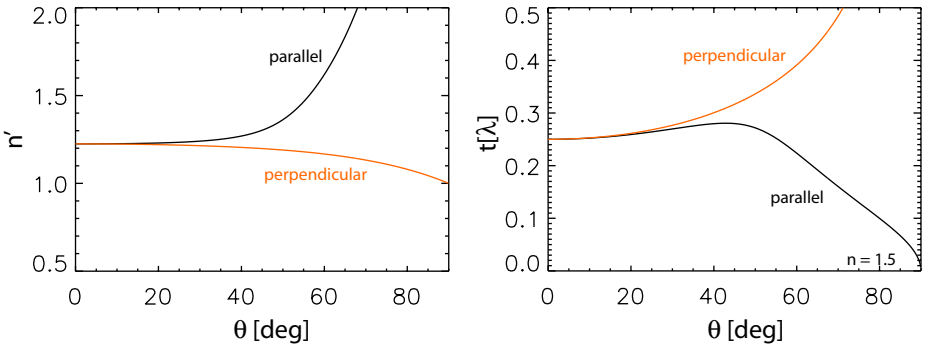

Figure 8. This figure shows the index of refection (left) and design thickness (right) of a $\lambda/4$ AR layer on HDPE as a function of angle of incidence for both linear polarization states (red and black curves). The thickness t is given in units of wavelength within the matching layer.

for light perpendicular to the plane of incidence. The thickness of the matching layer t is given by

$$t(\theta) = \frac{\lambda}{4\sqrt{n'^2 - \sin^2\theta}} \tag{3}$$

where n' is given by either Equation 1 or 2 depending on the choice of linear polarization. The dependance of n' and t on angle and linear polarization is shown in Figure 8 for the case of a substrate with $n = 1.5$. Note that the requirements for n' and t for the two linear polarization states diverge for $\theta > 30°$. Use of $\lambda/4$ AR layers at high angles of incidence suffer from reduced performance and lead to differences in the reflected power between linear polarization states generating cross-polarization. Application of $\lambda/4$ AR layers above about 30° should be avoided.

Wider bandwidth and greater immunity to the polarization dependance of boundary conditions at large angles of incidence can be achieved using graded-index AR coatings. Graded-index AR coatings consist of a dielectric layer over which the index of refraction varies approximately adiabatically between 1 and the index of the substrate n. The performance of these AR coatings improves with increases in the thickness of the layer, but offer a factor-of-two improvement even if the thickness is only $\lambda/4$ [31]. These coatings can suppress reflections below -25dB over $> 100\%$ bandwidth (see *University of Minnesota* in Section 5.3).

5.2. Description of Technology.

Both the $\lambda/4$ and graded-index coatings discussed in the previous section can be made using simulated dielectric techniques. An SD consists of a layer of dielectric which has been perturbed by removal of material (typically by simple machining) to form sub-wavelength structure. The geometry of these structures is chosen to tune the effective index of refraction n' of this layer to any value between the index of refraction of the substrate n and that of vacuum. Typical $\lambda/4$ SD-AR layers are made by cutting grooves, drilling periodic arrays of holes, or making an array of posts on the surface of the optic to be treated. See Figure 9 for examples.

An overview (summarized here) of the theory and performance of $\lambda/4$ SD-ARs can be found in [30]. Approximate analytic expressions for n' can be derived by calculating the polarizability of the SD layer when it is placed in a uniform electric field, treating the layer as infinitely thick, and neglecting the coupling between neighboring dielectric structures. Enforcing the condition $n' = \sqrt{n}$ yields equations for the 'fill factor' f needed for a quarter wave layer. These expressions depend on

θ, but at normal incidence reduce to

$$f_{g,\perp} = \frac{1}{n+1} \tag{4}$$

$$f_{g,||} = \frac{n}{n+1} \tag{5}$$

for grooves (light polarized perpendicular and parallel to grooves respectively), and

$$f_h = \frac{n^2+1}{2n(n+1)} \tag{6}$$

for holes. The required fill factor for posts has been experimentally found to be 0.88 of that of holes. We emphasize that grooves are birefringent ($f_{g,\perp} \neq f_{g,||}$) and therefore not suitable for polarization measurements. Holes and posts do not share this problem when placed on a square grid, though asymmetric grids can also lead to birefringence. These formula are accurate to $\approx 10\%$ provided the scale of the features are less than $\approx \lambda/2$.

Graded index SD-AR layers can be made by tapering the width of the grooves, cones, or posts. This amounts to cutting grooves with a triangular cross-section, drilling conical holes, or making square bottomed pyramids on the surface to be treated. This taper causes the fill factor (and therefore n') to vary with depth. It has also been proposed to make wide-band SD-ARs by drilling a large number of holes with uniformly distributed random locations and random depths chosen from a distribution such that the n' is appropriately tapered with depth in the layer. The bandwidth of such layers depends on both the thickness and taper of the index. Calculations of the performance of these layers are possible using electromagnetic simulators such as HFSS or by approximating the system as a cascade of thin layers of material with varying effective index. The latter calculation shows that the performance improves as the layer is made thicker and is only weakly dependent on the functional form of the taper[31]. The scale of features in these layers should be kept smaller than $\approx \lambda/2$.

5.3. Status of this Technology

Figure 9. Examples of SD layers from several groups: $\lambda/4$ grooves in HDPE from DASI, $\lambda/4$ holes in HDPE from CAPMAP, and an adiabatic transition consisting of tapered square posts in rexolite from the University of Minnesota.

In this section we note and briefly discuss SD-AR designs which have been used or considered by various groups in the CMB community. For each group we describe the geometry of the SD layer, summarize the performance (when possible), and note if the technology was fielded. The order of this list is roughly chronological.

DASI High density poly ethylene (HDPE) meniscus lenses were AR coated using a $\frac{1}{4}$-λ thick (at 32 GHz) SD layer consisting of concentric grooves. Measured reflections were below 1% across 30% bandwidth. The birefringence of these grooves lead to a peak cross-polarization of -22 dB. Published polarization science data were taken with this system.

CAPMAP Bi-convex lenses made from HDPE were AR coated using a $\frac{1}{4}$-λ thick SD layer consisting of a square grid of holes. Lenses were made for the 40 and 90 GHz band. Measured reflections were below 1% across 20% bandwidth in both cases. The measured cross-polarization of these lenses were below -40 dB. Published polarization science data were taken with this system.

SPT / APEX HDPE lenses were AR coated using a wide-band graded index SD layer consisting of concentric triangular grooves. The ratio of the width to depth of these grooves is 1:1. Measurements are not available, but simulations suggest that the peak transmission is 99% at 150 GHz with greater than 98% transmission between 100 and 300 GHz This design is not optimized for polarization science due to the birefringence of the grooves. This system is currently fielded.

University of Minnesota has prototyped a wideband SD-AR consisting of a square grid of square bottom pyramids (see Figure 9) on a flat Rexolite ($n \approx 1.5$) surface. The hight of the pyramids is 500 μm and the grid spacing is 250 μm. Calculations predict a reflectance of less than 0.2% over a band between 100 and 500 GHz. Noise-limited lab measurements at frequencies between 120 and 300 GHz using a Fourier transform spectrometer imply the reflection is less than $\approx 2\%$ over the entire bandwidth. No measurements of polarization purity are available.

UC Berkeley An attempt to mill a square grid of 4 : 1 (depth to width) square based pyramids on small samples of TMM (plastic) lenses was aborted due to difficulties with machining. Laser and EDM machining in Silicon were considered but not attempted.

Miller Group The Miller group at Columbia has considered micro-machining holes into a thin layer of silicon and 'slumping' this SD layer onto a silicon optic. This approach is expected to work on a flat substrate, but is believed to be more difficult than direct machining.

5.4. Benefits and Disadvantages.

The benefits of this technology are 1) its mechanical robustness, 2) ability to achieve arbitrary index of refraction, and 3) automatic matching of the CTE of the AR layer to the CTE of the lens. For SD layers which are highly symmetric, low-cross polarization has been demonstrated. The disadvantage of this technology is that its applicability is limited to materials that can be machined appropriately (currently HDPE, LDPE and Rexolite). The implications of this restriction depend on the design of the full optical system. If high magnification lenses are required this restriction could be a severe disadvantage while for designs using plastic lenses this is not an issue. It is likely that direct machining of silicon could be developed with some amount of experimentation.

5.5. Technical Readiness: Estimates for Time to TRL 5

The TRL level varies for the different SD designs with different materials. Designs using $\lambda/4$ SD-AR layers consisting of grooves and holes on HDPE have been used in CMB polarization experiments and achieved TRL 5. Wide band tapered designs (grooves in LDPE, pyramids in flat rexolite) have been prototyped, but have not yet been fielded in CMB polarization experiments. These designs are at TRL 4. Use of SD layers on silicon are TRL 2.

Several steps required to bring a new application of SD technology to TRL5. Electromagnetic simulations are the natural starting point. These could be completed in one to two man-months. The new application will then need to be fabricated. Changing materials or SD geometry will require extra time for development of appropriate machining techniques. For plastics, fabrication is likely to require several man months. For silicon this could easily require a year or more of development. Once a prototype has been fabricated several measurements are needed to verify its

performance. These measurements include 1) transmission and reflection, and 2) cross-polarization. The transmission and reflection measurements can be made using either a Fourier transform spectrometer or a network analyzer. Cross-polarization measurements could be made by measuring the transmission of the SD layer while rotating the sample or using beam measurements using a polarized (or strictly unpolarized) point source. These measurements could be completed in a few man-months at a well equipped facility, but would require more time if the test equipment needs to be acquired and set up.

Acknowledgments
I want to thank the members of the CMB groups listed in Section 5.3 for providing detailed information about the design and status of their SD-AR layers.

6. Bibliography

[1] Colombo L and The SPOrt Collaboration 2004 *Nuclear Physics B Proceedings Supplements* **134** 133–135
[2] Bock J, Cooray A, Hanany S, Keating B, Lee A, Matsumura T, Milligan M, Ponthieu N, Renbarger T and Tran H 2008 *ArXiv e-prints* **805** (*Preprint* 0805.4207)
[3] Timbie et al *EPIC Interferemoter Study*
[4] Newburgh L B, UC B C, Caltech Collaboration, Columbia U Collaboration, GSFC Collaboration, Harvard-Smithsonian CfA Collaboration, JPL Collaboration, Kavli Inst U C C, Kavli Inst S U C, U Miami Collaboration, U Oxford Collaboration and Princeton U Collaboration 2005 *Bulletin of the American Astronomical Society* pp 1429–+
[5] Taylor A C, Challinor A, Goldie D, Grainge K, Jones M E, Lasenby A N, Withington S, Yassin G, Gear W K, Piccirillo L, Ade P, Mauskopf P D, Maffei B and Pisano G 2004 *ArXiv Astrophysics e-prints* (*Preprint* astro-ph/0407148)
[6] Tran H, Hanany S, Lee A, Milligan M and Renbarger T 2008 *Appl. Opt.* 103–109 (*Preprint* ttp://www.opticsinfobase.org/abstract.cfm?URI=ao-47-2-103)
[7] Page L, Jackson C, Barnes C, Bennett C, Halpern M, Hinshaw G, Jarosik N, Kogut A, Limon M, Meyer S S, Spergel D N, Tucker G S, Wilkinson D T, Wollack E and Wright E L 2003 *Ap. J.* **585** 566–586 (*Preprint* arXiv:astro-ph/0301160)
[8] Hill R S, Weiland J L, Odegard N, Wollack E, Hinshaw G, Larson D, Bennett C L, Halpern M, Page L, Dunkley J, Gold B, Jarosik N, Kogut A, Limon M, Nolta M R, Spergel D N, Tucker G S and Wright E L 2008 *ArXiv e-prints* **803** (*Preprint* 0803.0570)
[9] Barnes C, Limon M, Page L, Bennett C, Bradley S, Halpern M, Hinshaw G, Jarosik N, Jones W, Kogut A, Meyer S, Motrunich O, Tucker G, Wilkinson D and Wollack E 2002 *Astrophysical Journal Supp* **143** 567–576 (*Preprint* astro-ph/0301159)
[10] Page L, Hinshaw G, Komatsu E, Nolta M R, Spergel D N, Bennett C L, Barnes C, Bean R, Doré O, Dunkley J, Halpern M, Hill R S, Jarosik N, Kogut A, Limon M, Meyer S S, Odegard N, Peiris H V, Tucker G S, Verde L, Weiland J L, Wollack E and Wright E L 2007 *Ap. J. Suppl.* **170** 335–376 (*Preprint* arXiv:astro-ph/0603450)
[11] Villa F, Sandri M, Bersanelli M, Butler R C, Mandolesi N, Mennella A, Marti-Canales J and Tauber J 2003 *ArXiv Astrophysics e-prints* (*Preprint* astro-ph/0304137)
[12] Yurchenko V B, Murphy J A and Lamarre J M 2004 *Optical, Infrared, and Millimeter Space Telescopes. Edited by Mather, John C. Proceedings of the SPIE, Volume 5487, pp. 542-549 (2004).* (*Presented at the Society of Photo-Optical Instrumentation Engineers (SPIE) Conference* vol 5487) ed Mather J C pp 542–549
[13] Noviello F 2006 *CMB and Physics of the Early Universe*
[14] Rosset C, Yurchenko V B, Delabrouille J, Kaplan J, Giraud-Héraud Y, Lamarre J M and Murphy J A 2007 *Astron. Astrophys.* **464** 405–415
[15] Yurchenko V and Altintas A 2007 *Proc. 6th Intl. Conf. on Antenna Theory and Techniques (ICATT'07)*
[16] Dragone C 1982 *IEEE Transactions on Antennas and Propagation* **30** 331–339
[17] Hanany S and Marrone D P 2002 *Applied Optics* **41** 4666–4670
[18] Farese P C, dall'Oglio G, Gundersen J, Keating B, Klawikowski S, Knox L, Levy A, O'dell C, Peel A, Piccirillo L, Ruhl J and Timbie P 2003 *New Astronomy Review* **47** 1033–1046 (*Preprint* arXiv:astro-ph/0305608)
[19] Hinderks J, Ade P, Bock J, Bowden M, Brown M L, Cahill G, Carlstrom J E, Castro P G, Church S, Culverhouse T, Friedman R, Ganga K, Gear W K, Gupta S, Harris J, Haynes V, Kovac J, Kirby E, Lange A E, Leitch E, Mallie O E, Melhuish S, Murphy A, Orlando A, Schwarz R, O' Sullivan C, Piccirillo L, Pryke C, Rajguru N, Rusholme B, Taylor A N, Thompson K L, Tucker C, Wu E Y S and Zemcov M 2008 *ArXiv e-prints* **805** (*Preprint* 0805.1990)

[20] Pryke C, Ade P, Bock J, Bowden M, Brown M L, Cahill G, Castro P G, Church S, Culverhouse T, Friedman R, Ganga K, Gear W K, Gupta S, Hinderks J, Kovac J, Lange A E, Leitch E, Melhuish S J, Memari Y, Murphy J A, Orlando A, Schwarz R, O'Sullivan C, Piccirillo L, Rajguru N, Rusholme B, Taylor A N, Thompson K L, Turner A H, Wu E Y S and Zemcov M 2008 *ArXiv e-prints* **805** (*Preprint* 0805.1944)
[21] Born M and Wolf E (eds) 1999 *Principles of optics : electromagnetic theory of propagation, interference and diffraction of light*
[22] Lamb J W 1996 *International Journal of Infrared and Millimeter Waves* **17** 1997–2034
[23] Lau J e a 2006 *Applied Optics* **45**
[24] Stycast 1266 *Emerson and Cuming, 869 Washington Street, Canton, MA 02021*
[25] Yoon K W, Ade P A R, Barkats D, Battle J O, Bierman E M, Bock J J, Brevik J A, Chiang H C, Crites A, Dowell C D, Duband L, Griffin G S, Hivon E F, Holzapfel W L, Hristov V V, Keating B G, Kovac J M, Kuo C L, Lange A E, Leitch E M, Mason P V, Nguyen H T, Ponthieu N, Takahashi Y D, Renbarger T, Weintraub L C and Woolsey D 2006 *Millimeter and Submillimeter Detectors and Instrumentation for Astronomy III. Edited by Zmuidzinas, Jonas; Holland, Wayne S.; Withington, Stafford; Duncan, William D.. Proceedings of the SPIE, Volume 6275, pp. 62751K (2006).* (*Presented at the Society of Photo-Optical Instrumentation Engineers (SPIE) Conference* vol 6275)
[26] Benford D J, Gaidis M C and Kooi J W 2003 *Applied Optics* **42** 5118–5122
[27] Jackson J D 1975 *Classical electrodynamics* (New York: Wiley, 1975, 2nd ed.)
[28] Fralock, Division of Lockwood Industries, Inc *21054 Osborne Street, Canoga Park, CA 91304.*
[29] Chemlok AP-134 *Lord Corporation, 111 Lord Drive, P.O. Box 8012, Cary, NC 27512*
[30] Cohn S B 1961 *Lens Type Radiators: Antenna Engineering Handbook* (McGraw-Hill, N.Y.)
[31] Plagge T 2008 *tplagge@berkeley.edu, private comunication*